nature geoscience

SUPPLEMENTARY INFORMATION

https://doi.org/10.1038/s41561-017-0006-3

In the format provided by the authors and unedited.

Oxygenation as a driver of the Great Ordovician Biodiversification Event

Cole T. Edwards[1]*, Matthew R. Saltzman[2], Dana L. Royer[3] and David A. Fike[4]

[1]Department of Geological and Environmental Sciences, Appalachian State University, Boone, NC, USA. [2]School of Earth Sciences, The Ohio State University, Columbus, OH, USA. [3]Department of Earth and Environmental Sciences, Wesleyan University, Middletown, CT, USA. [4]Department of Earth and Planetary Sciences, Washington University in St. Louis, St. Louis, MO, USA. *e-mail: edwardsct4@appstate.edu

Oxygenation as a driver of the Great Ordovician Biodiversification Event

Supplementary Information

Cole T. Edwards, Matthew R. Saltzman, Dana L. Royer, and David A. Fike

Model sensitivity testing

GEOCARB

New O_2 estimates using the GEOCARB model are broadly similar to previous GEOCARB results[33] with the important exception of an O_2 increase during the Middle and Late Ordovician (Fig. S1). We established reasonable uncertainties for the three new isotope datasets used in our standard GEOCARB run. For each dataset (Sr, C, and S) and the other 65 inputs, we reduce the measured uncertainties (Fig. 1) in all time bins proportionately, resampling only one dataset at a time (and leaving all other inputs fixed), until failure rates in all time bins are less than 5%, following ref. *33*. Our reported uncertainties (light gray band in Fig. 2) are likely too large because the model failure rate in the fully propagated run is high (~85%), meaning that many combinations of input value choices are incompatible with the model[33]. Uncertainties for Sr, C, and S required reductions of 0, 83, and 88%, respectively, to achieve <5% failure for all time bins. One exception, however, is that time bin 465 Ma consistently has failure rates of 65–99% caused by a low $\delta^{13}C$ mean value of –1.42‰ in the 470 Ma time bin. Increasing $\delta^{13}C$ to ~ –1.2‰ causes model failure rates to be <5% for all time bins. After this $\delta^{13}C$ adjustment, when all inputs are resampled simultaneously, the highest failure rates in the standard GEOCARB run occur in the 465 Myr time bin (89%; Table S1). Because failure rates are generally high in our standard run, we carry out 100,000 Monte Carlo simulations in order to ensure > 10,000 successful individual runs.

The sulfur isotope data used in the standard GEOCARB run are the least constrained with respect to data density and age resolution relative to the $\delta^{13}C_{carb}$ and $^{87}Sr/^{86}Sr$ records (Fig. 1). Our standard GEOCARB run (Fig. 2) uses high-resolution $\delta^{34}S$

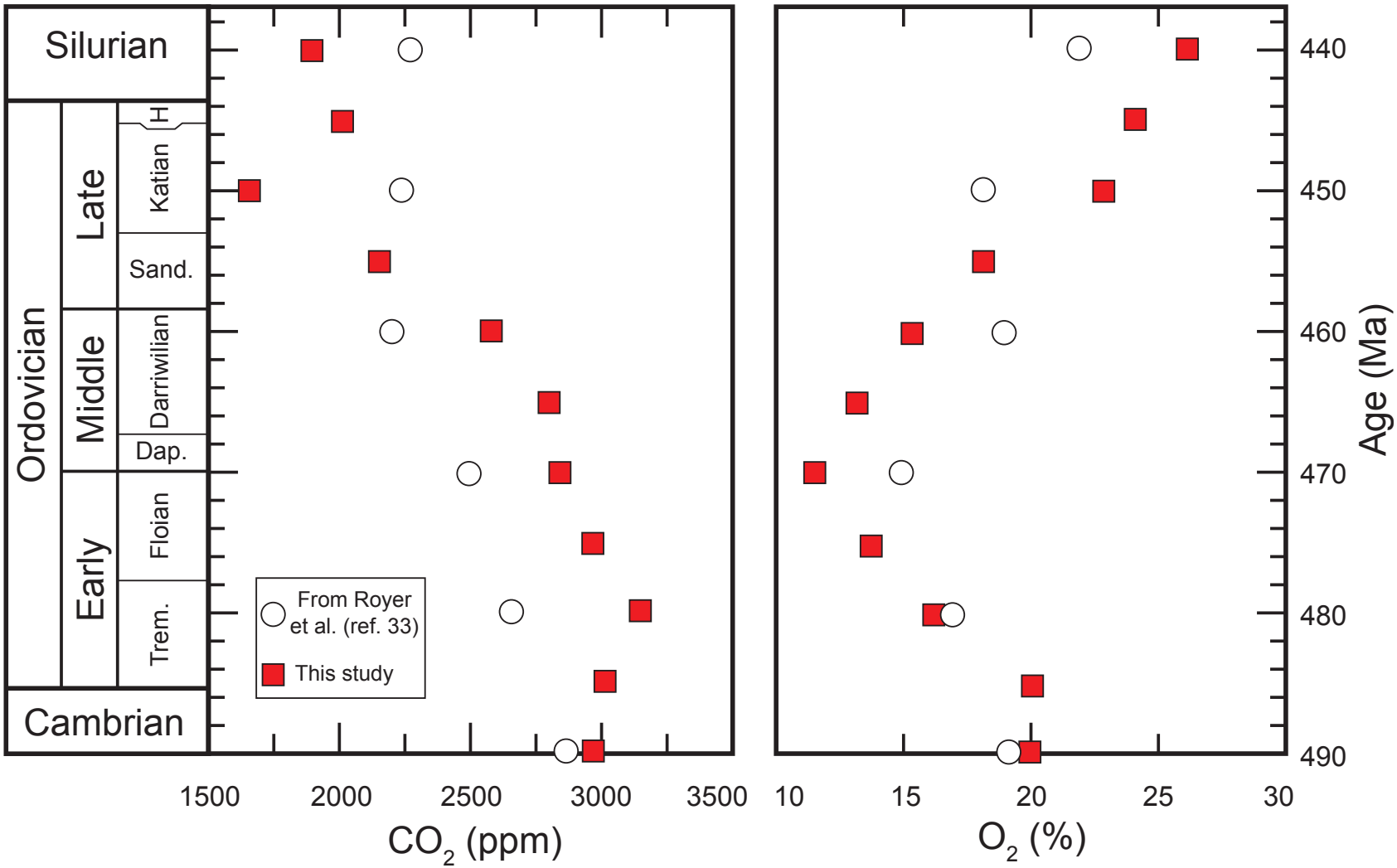

Edwards et al., Figure S1

data from a single stratigraphic section (Shingle Pass, NV[49]) with values that are similar to what is thought to be the global $\delta^{34}S$ trend[47].

Sensitivity testing of GEOCARB by holding each updated dataset ($\delta^{13}C$, $\delta^{34}S$, and $^{87}Sr/^{86}Sr$) constant individually shows that constant $\delta^{34}S$ values result in overestimates of O_2 during the Middle Ordovician compared to other model runs, but the Middle–Late Ordovician increase is still evident (Fig. S2). Our model run with constant $\delta^{13}C$ does estimate that atmospheric O_2 was <15% during the Middle Ordovician, but in this case the Middle–Late Ordovician oxygenation is not evident. These sensitivity tests suggest that the combination of observed $\delta^{13}C$ and $\delta^{34}S$ trends does in fact play an important role in O_2 estimates where neither input alone is responsible for driving the GEOCARB O_2 estimates. Likewise, holding each of these parameters constant does not appreciably affect CO_2 estimates (Fig. 2), which is particularly important because $\delta^{13}C_{carb}$ data are used in both approaches and does not appear to affect the non-independence of the models. In the model's base run the GEOG parameter increases during the time of the CO_2 drop, which accounts for changes in temperature relative to today[33] and should impact silicate weathering rates (a CO_2 sink). Holding this term constant at 490 Ma does decrease the magnitude of the CO_2 drop, suggesting that weathering rates and temperature are largely what are driving this CO_2 drop and not variations in the updated $\delta^{13}C$ and $^{87}Sr/^{86}Sr$ records.

Photosynthetic fractionation effect model

Using the $\varepsilon_{p\text{-estimated}}$ trend and Eq. 3, atmospheric O_2 levels can be calculated after removing the effect of variations in CO_2 ($\varepsilon_{p\text{-expected}}$) and scaled using an empirically

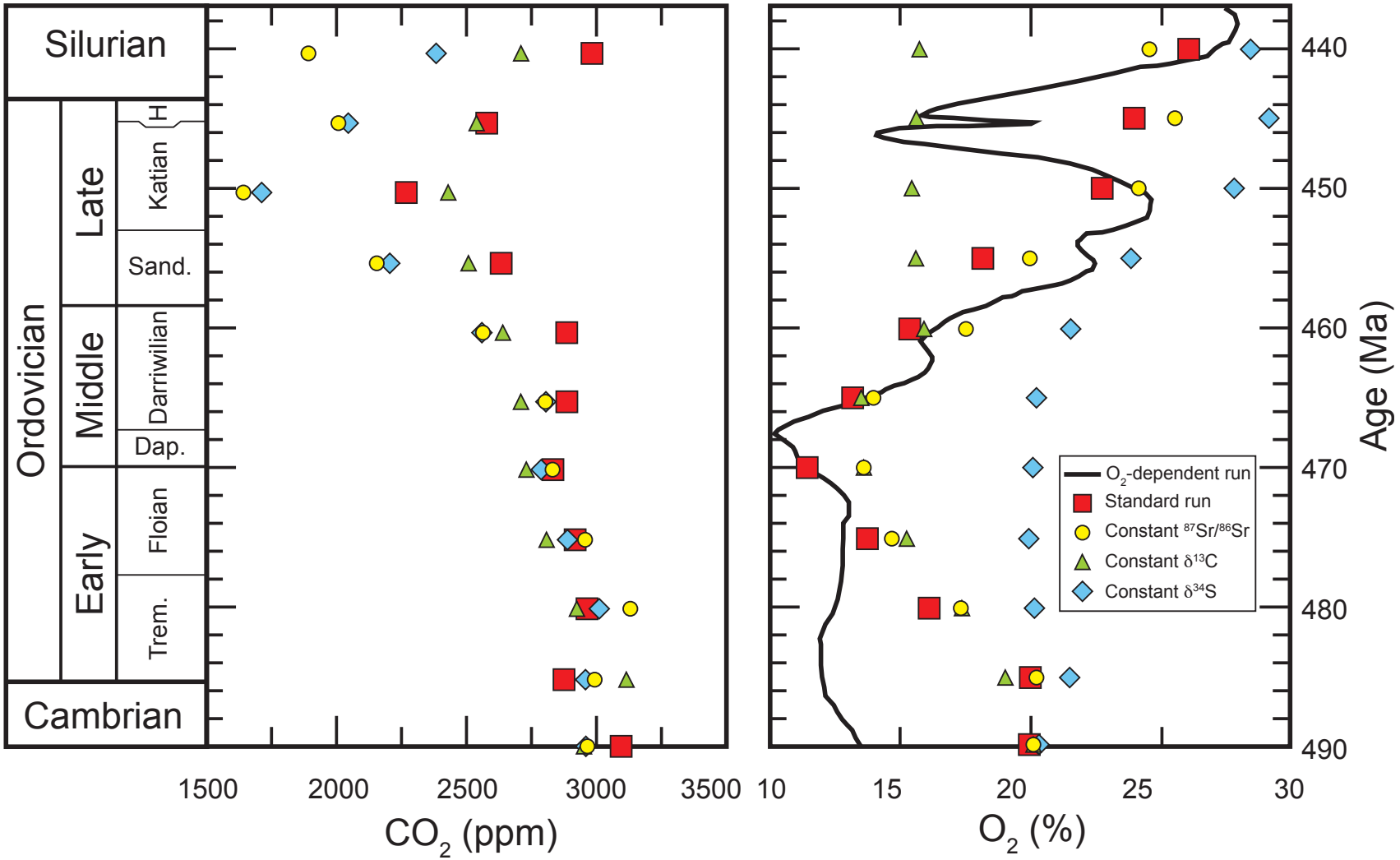

Edwards et al., Figure S2

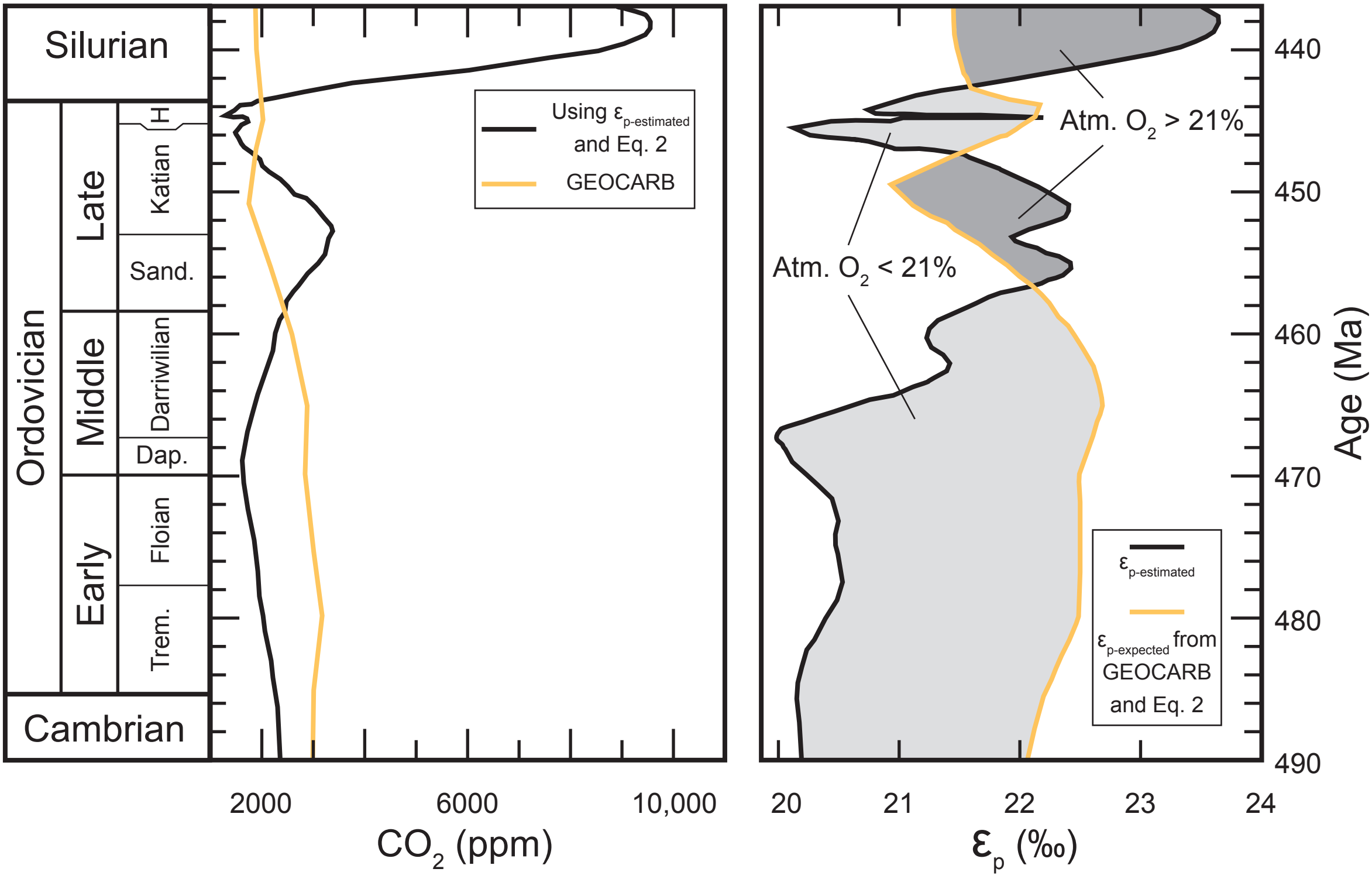

Edwards et al., Figure S3

derived value (J). The parameter J describes the dependence of isotopic fractionation on estimated O_2. Using J = 2.5, as in ref. 22, yields very low O_2 values <5% during the Early–Middle Ordovician (~485–467 Myr) and very high O_2 (>25%) just 15 Myr later (Fig. S4A). Saltzman et al. (ref. 58) also found that small J values yield unrealistic atmospheric O_2 values during the late Cambrian. When a larger value is used (J = 7.5), the same O_2 patterns are present but they are dampened (Fig. S4A). We favor using a value for J =5 because it is close to what other studies have used to model Paleozoic atmospheric O_2 (2.5–5)[16,58,59] and because it does not lead to highly improbable swings in estimated O_2.

Despite using a similar J value, individual calculated O_2 values exhibit significant scatter between successive measurements, including some negative O_2 values (Fig. S5). We pass a LOESS smoothing line throughout all calculations to capture the overall O_2 trend. When O_2 calculations are binned in a similar resolution to GEOCARB estimates (blue circles in Fig. S5), the Hirnantian O_2 drop is still present, suggesting that either the O_2-dependent fractionation approach is capturing a short-term change in the carbon cycle not capable of being resolved in the GEOCARB model (consistent with the <1 Myr estimated duration of the Hirnantian $\delta^{13}C$ excursion), or this drop is an artifact related to uncertainties in $\delta^{13}C$ correlation across several datasets with poor biostratigraphic age resolution.

A close examination of the data used to derive O_2 estimates using the photosynthetic fractionation approach shows that a small, but resolvable increase in $\delta^{13}C_{org}$ is driving lower $\varepsilon_{p\text{-estimated}}$ values (Fig. S6). $\delta^{13}C$ data collected from Anticosti Island[42,43], calibrated to the 2012 Geologic Time Scale using graptolite and chitinozoan

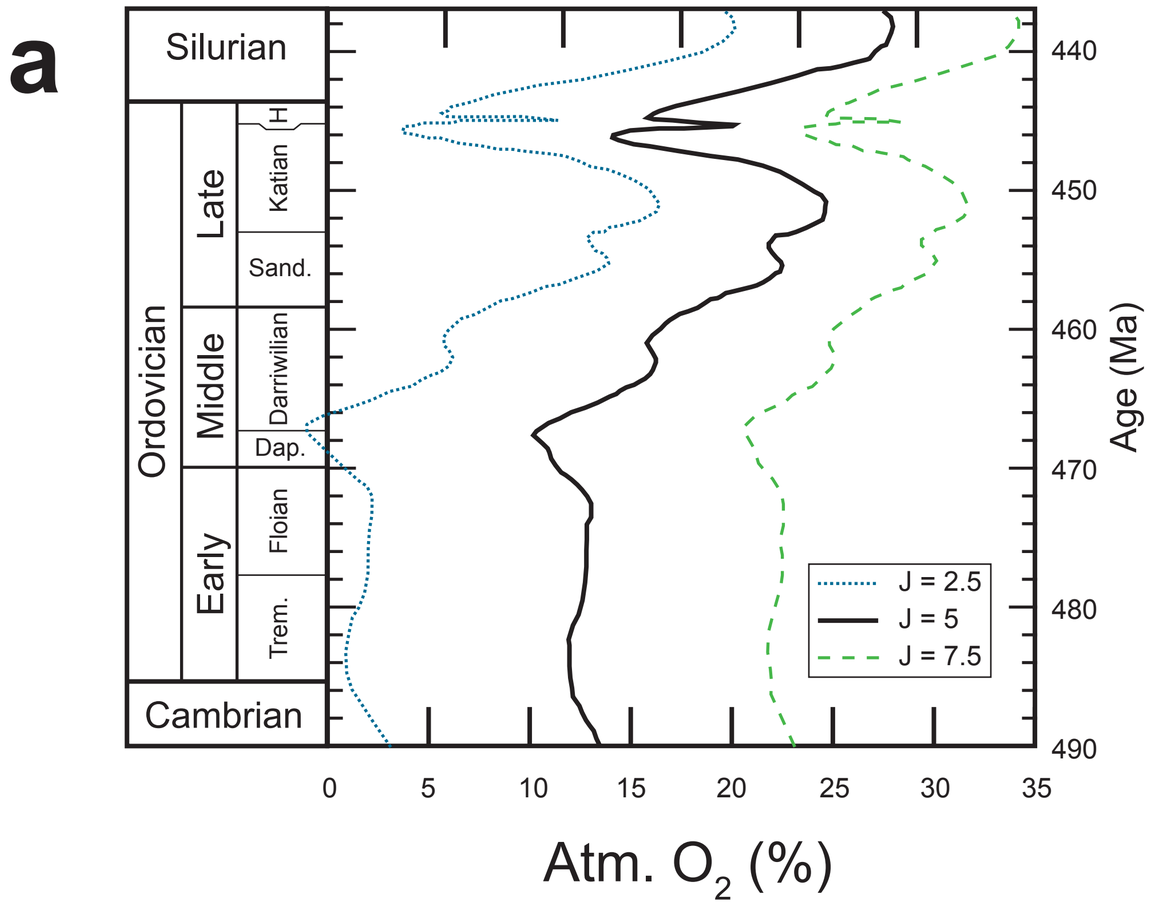

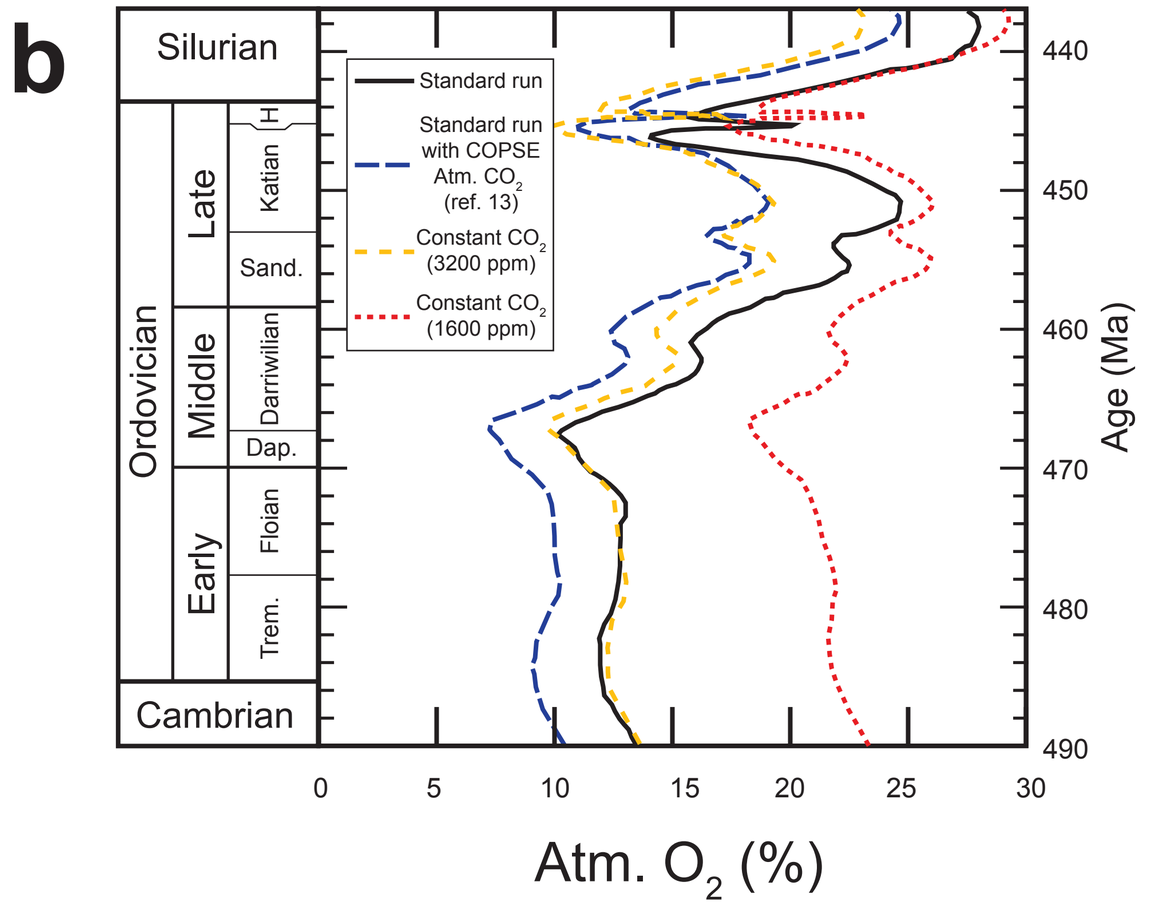

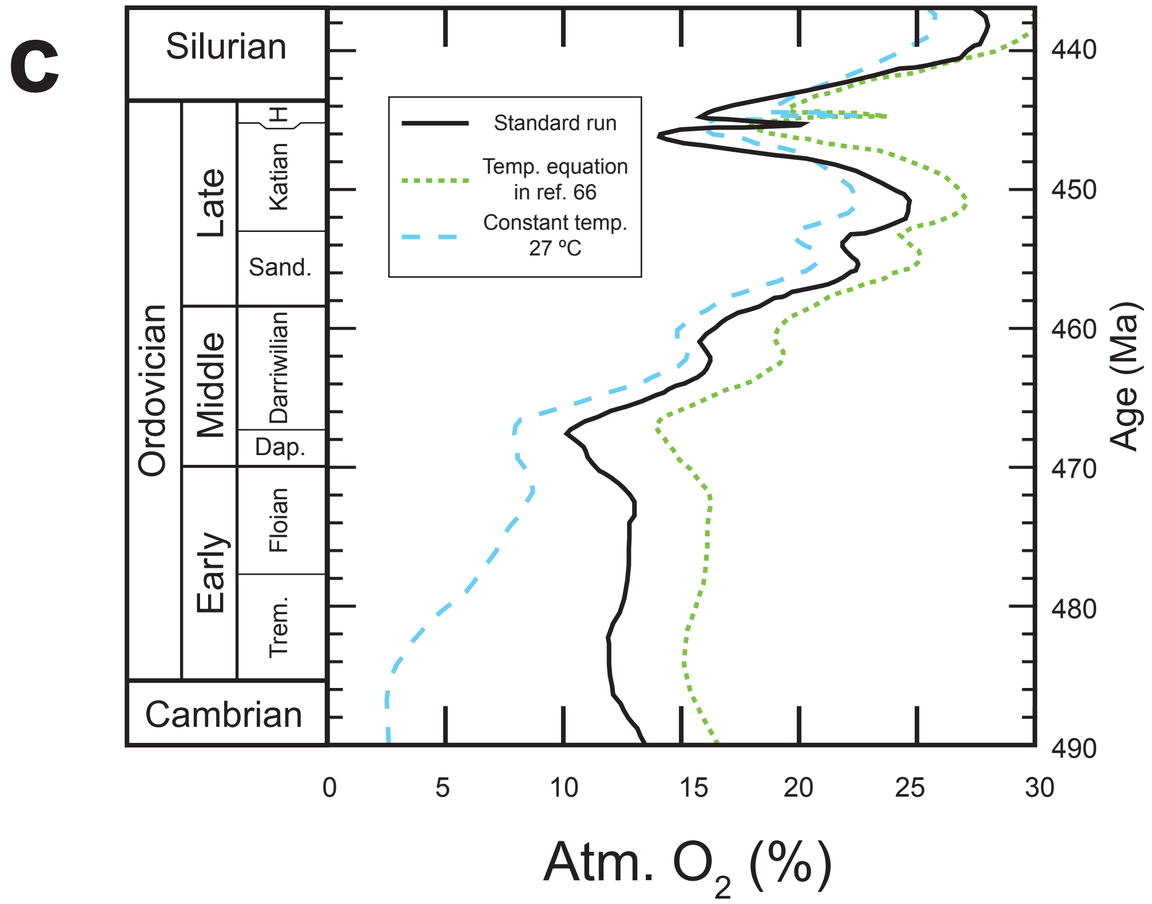

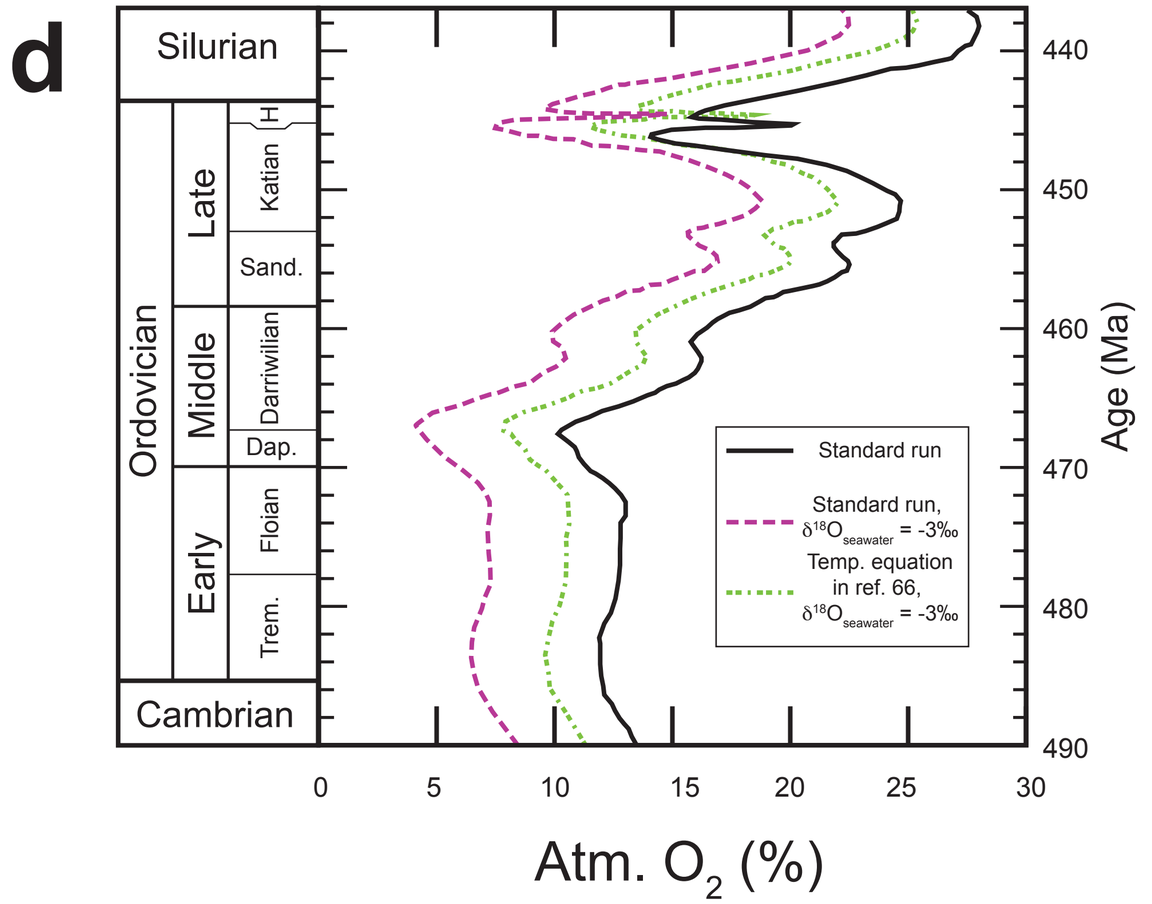

Edwards et al., Figure S4

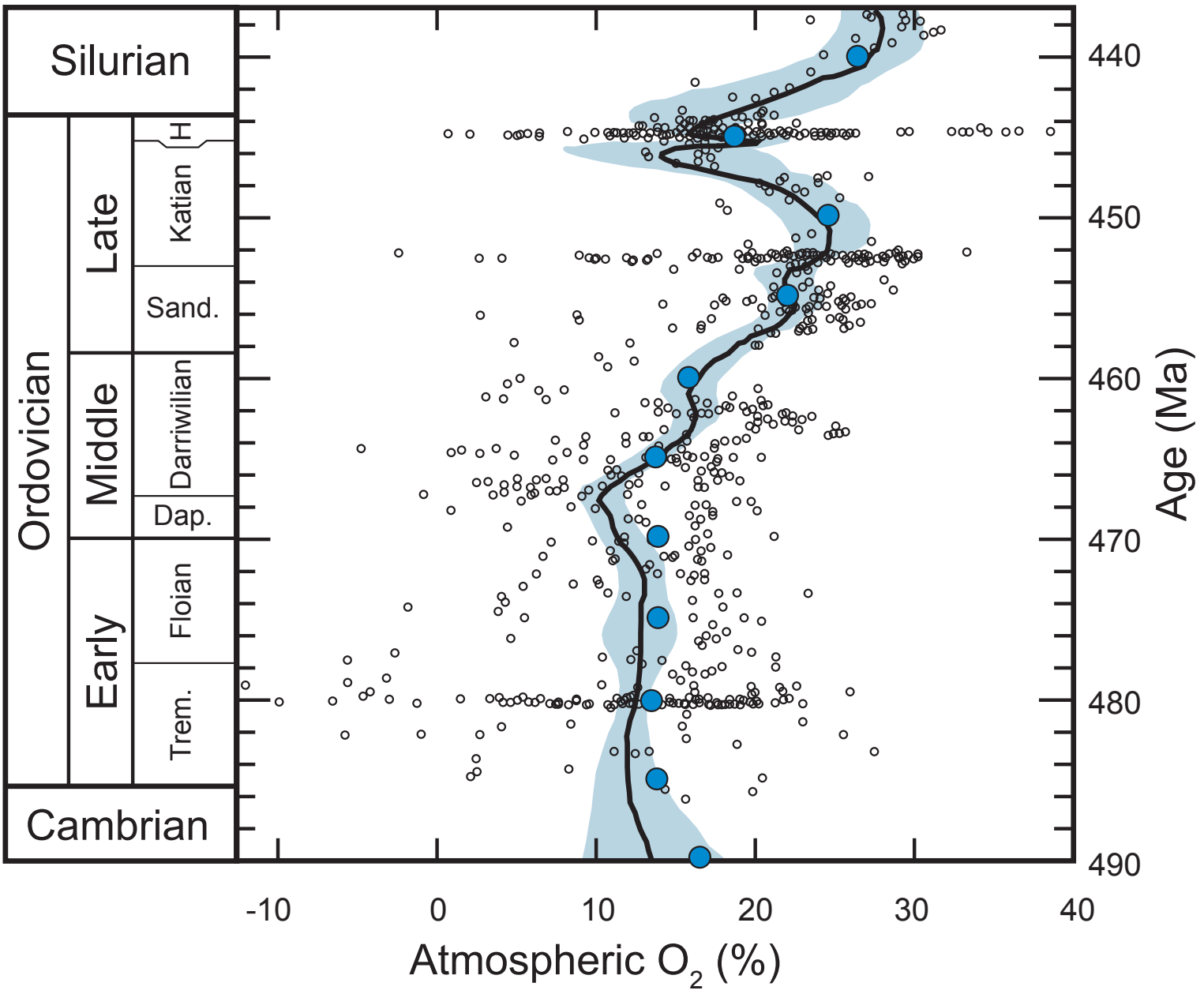

Edwards et al., Figure S5

biozones, both indicate that O_2 decreased prior to the HICE event. O_2 estimates based on $\delta^{13}C$ data from Nevada[52], using just graptolite biozones for age calibration, also shows an O_2 drop prior to the HICE event. However, this drop occurs prior to the O_2 drop using Anticosti Island data (Fig. S6) and does not drop much below near-modern O_2 levels (21%). It may be possible that all three sections record the same O_2 drop prior to the Hirnantian glaciation and mass extinction event, but until more highly resolved biostratigraphic information becomes available from these (and other) Hirnantian sections we only want to point out the possibility that an oxygen crisis may have occurred, which we hope will encourage future investigation into this time period.

Modeling atmospheric O_2 during other periods of Earth history: limitations and directions for continued study

The models used in this study could be used to explore variations in atmospheric O_2 levels during other times of Earth history, such as the Mesozoic ocean anoxic events (OAEs). During Mesozoic OAEs $\delta^{13}C$ and $\delta^{34}S$ have been shown to fluctuate over the course of 1–2 Myr, interpreted to transiently record marine anoxia or euxinia in shallow environments[60,61]. These isotopic excursions would be averaged out to a single input parameter in a 5 Myr time bin of GEOCARB, which is unlikely to show any significant change in O_2 and prevents a meaningful comparison of O_2 estimates between the models used here. Conceptually, the photosynthetic effect approach has the potential to record changes in atmospheric O_2, provided high-resolution paired $\delta^{13}C$ measurements and atmospheric CO_2 estimates exist. Nevertheless, given that these OAEs occurred during times of major change to biogeochemical cycles, it is possible that local algal

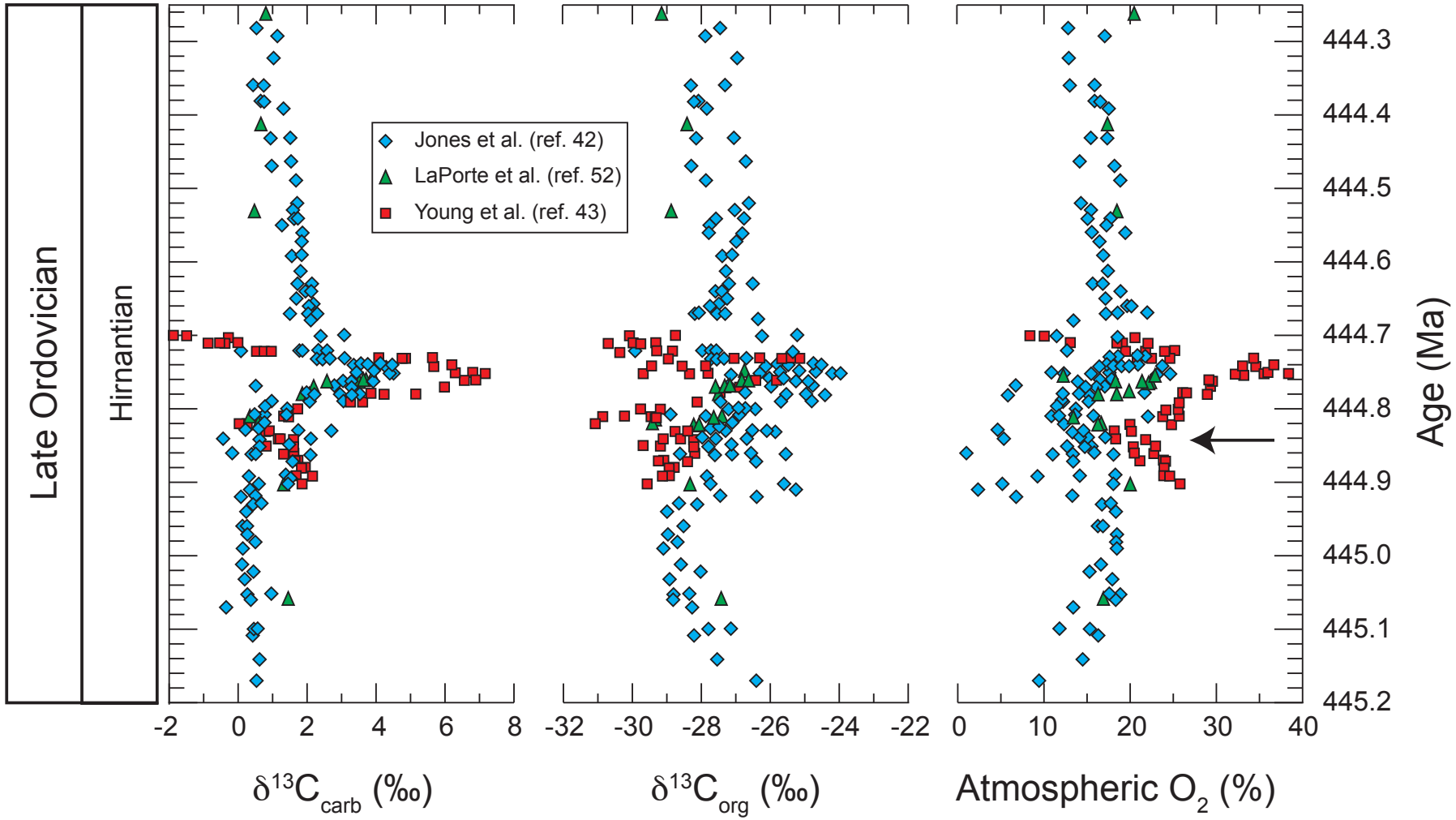

Edwards et al., Figure S6

assemblages were also physiologically affected (if not completely replaced by new populations). Thus, caution should be used when interpreting any short-term changes in $\varepsilon_{p\text{-estimated}}$ values as they may instead record temporary changes to biological controls (growth rates, cell size, new dominant groups that have unique 'vital effects') instead of atmospheric O_2 variation.

Applying this photosynthetic fractionation approach to the post-Eocene interval is also not likely to yield atmospheric O_2 levels similar to GEOCARB (or other independent means to estimate O_2 levels). The alkenone community has struggled to use ε_p measurements from Cenozoic coccolithiphore biomass as a proxy for paleoclimate trends, without factoring in cell size and vital effects[62,63]. These algae, among others, are known to utilize carbon-concentrating mechanisms (CCMs) during periods of low atmospheric CO_2, which discriminate ^{12}C differently compared other algal groups and will yield different ε_p values under similar CO_2 and O_2 levels. Although Cenozoic strata contain high-resolution $\delta^{13}C$ trends from well-preserved bulk and compound-specific organic molecules, because CCMs were likely used by some algae included in bulk records $\varepsilon_{p\text{-estimated}}$ values are not likely to strictly record changes in atmospheric CO_2 or O_2. Thus, using $\varepsilon_{p\text{-estimated}}$ values from the post-Eocene to modern in our photosynthetic fractionation approach will not produce similar O_2 estimates with GEOCARB.

Error analysis and error propagation calculations

Error analysis and uncertainties for atmospheric CO_2 and O_2 values using GEOCARB (Table S1) are calculated using the original code, discussed in detail in Royer et al. (ref. 33). Uncertainties for O_2 estimates using the O_2-dependent fractionation effect approach

124 are determined using standard error propagation equations for each calculation. Table S5
125 shows an example of error propagation calculations, which includes a data value and its
126 error estimate (measured or calculated using a particular error propagation calculation;
127 the example shown is the first row in Table S2). Error propagation calculations were
128 compared against Monte Carlo simulations (bottom portion of table) to check that
129 reasonable uncertainties were calculated. Error analysis using Monte Carlo simulations
130 was done by generating 10,000 random values using the inverse of the cumulative normal
131 distribution (NORMINV function in Excel®) and the value's associated uncertainty. The
132 median value of these 10,000 randomly generated values was treated as the calculated
133 value (e.g. 1845 for 'Interpolated pCO_2 (ppm)'), and 1σ was calculated by subtracting the
134 median value from the 84th percentile value. The 95% confidence interval of the
135 smoothed LOESS line in Figure 2 was produced using 'predict function' in R Studio®,
136 which does not depict the error associated with each data point from Table S2. This is
137 not meant to dismiss the large uncertainties associated with each value; rather we
138 emphasize the confidence of the long-term trend based on the large dataset used here.
139
140 **Controls on $\Delta^{13}C$:**
141 The main control on $\Delta^{13}C$ is the biological fractionation effect (ε_p), but temperature
142 during carbonate formation and secondary heterotrophy of organic matter (Δ_2) can also
143 play an important role (Fig. S7; ref. 25). Temperature has a strong effect on the isotopic
144 fractionation (0.12‰/ºC) between aqueous CO_2 ($[CO_2]_{aq}$) in the surface ocean and the
145 dissolved inorganic carbon (DIC) reservoir (represented by the term Δ_{carb} in Fig. S7).
146 There is a small temperature effect (0.01‰/ºC) associated with the formation of

Table S5. Example calculations for error propagation using the O_2-dependent photosynthetic fractionation approach.

Error propagation calculations (blue cells)																									
Age	**$\delta^{13}C_{carb}$**	**σ***	**$\delta^{13}C_{org}$**	**σ***	**Interpolated pCO_2 (ppm)**	**σ#**	**Interpolated Temperature (ºC)**	**σ#**	**T (K)**	**Ko**	**$[CO_2(aq)]$ mol/L/atm**	**σ%**	**E_{ba}**	**σ%**	**ε_p without 1.5‰ ^{13}C enrichment**	**σ&**	**ε_p - expected from pCO_2**	**σ$**	**pO_2 effect (‰)**	**σ§**	**Estimated O_2 (mol x 10^{18})**	**σ%**	**Estimated pO_2 (%)**	**σ$**	**2σ**
433.47	3.41	0.1	-26.69	0.20	1851	805	30	2.2	303	0.0257	47.62	20.71	-8.42	0.24	22.82	0.43	21.41	1.56	1.41	1.62	48.71	12.30	25.5	6.66	13.32
Error analysis by Monte Carlo simulations (blue cells)																									
433.47	3.23	0.10	-27.08	0.20	1845	813	30.0	2.2	303	0.0257	48.25	20.35	-8.43	0.23	21.01	0.34	21.47	1.06	1.38	2.60	48.48	19.27	25.52	7.09	14.18

* Typical analytical error for these measurements

\# Interpolated σ between time bins from GEOCARB output

% Using multiplication rules for error propagation of a constant (4.38) from temperature conversion equation in Trotter et al. (ref. 6), multiplied by average analytical error for $\delta^{18}O$ measurements

& Error propagation rule/equation: Multiplication of uncertainties

@ Error propagation rule/equation: Exponents, addition, and multiplication, with a constant, of uncertainties

$ Error propagation rule/equation: Multiplication, with a constant, of uncertainties

§ Error propagation rule/equation: Addition of uncertainties

148 carbonate from seawater, but this effect is outweighed by the 1‰ depletion between
149 carbonate formation from the DIC[25]. In most marine environments Δ_{carb} can vary by up
150 to 3.4‰ due to temperature effects alone between 30 ºC (8.2‰) and 0 ºC (11.6‰).
151 Secondary processes (Δ_2) associated with the metabolic breakdown (heterotrophy)
152 of organic matter from primary producers can also influence $\Delta^{13}C$. Studies of modern
153 environments underlying upwelling zones show that sedimentary organic matter can be
154 enriched in ^{13}C by as much as 3.5‰ compared to primary biomass, with a typical mean
155 value of +1.5‰ based on observations from a range of oxic environments (ref. 25 and
156 references therein). Negative Δ_2 values can result when a portion of the original biomass
157 is replaced by biomass from anaerobic chemoautotrophic organisms. This difference can
158 be as much as 3‰ between the $\delta^{13}C$ of biomass from photosynthesizers ($\delta^{13}C_{org}$: ~ –
159 22.5‰) versus sulfur-oxidizers ($\delta^{13}C_{org}$: ~ –25.5‰) as measured in the modern dysoxic
160 Black Sea [64]. However, our study areas are interpreted as well-oxygenated shallow
161 marginal and epicontinental seas (ref. 25 and refs. therein); thus, we exclude the
162 possibility for negative Δ_2 values. Together, we do not consider that changes in the
163 secondary alteration of organic matter over the duration of the Early–Middle Ordovician
164 can explain a 3‰ increase in $\Delta^{13}C$ (26 to 29‰), but we correct all $\delta^{13}C_{org}$ values by -
165 1.5‰ to more accurately estimate ε_p (eq. S3, see below). Hayes et al. (ref. 25) estimate
166 that a ^{13}C-enrichment of 1.5‰ of original biomass (δ_p) is representative of oxic marine
167 settings up to 100 cm deep into the sediment profile where a balance of secondary
168 processes favors a slight ^{13}C enrichment of bulk organic matter. Using these assumptions
169 about secondary microbial processes and carbonate formation, we can use paired $\delta^{13}C_{carb}$

and $\delta^{13}C_{org}$ measurements to estimate the $\delta^{13}C$ of dissolved CO_2 ($\delta^{13}C_{CO2}$) and primary biomass ($\delta^{13}C_{biomass}$), respectively, in order estimate ε_p (Fig. S7).

Determining ε_p values

Experimental work with modern phytoplankton shows that ε_p can be affected by biological effects and CO_2 partial pressure[22]. Cellular growth rates (μ) and volume/surface area (V/S) ratios influence ε_p such that the highest ε_p values are produced with slow growth rates or small V/S ratios. If these biological factors were solely responsible for the long-term increase in ε_p from 20.2‰ to 22.5‰ (Fig. S3), using Eq. 1 in Naafs et al. (ref. 31) would require the μ-V/S product to decline from 2.45 to 1.79 (where atmospheric CO_2 concentrations decrease from 2978 ppm to 2148 ppm during the increase in ε_p from 20.2‰ to 22.5‰) given the range of atmospheric CO_2 estimates from GEOCARB (A in Fig. S8). A typical μ-V/S product, however, of small modern marine algae only varies between 0.54 and 0.56 in two diatom species to as much as 0.88 in some haptophytes with slow growth rates (ref. *21* and refs. within). Some of the highest observed μ-V/S products (1.1–2.2) occur in highly productive upwelling zones where phytoplankton have large V/S ratios (2.2) but also have high growth rates (i.e. high μ: 0.5–1). Therefore it seems unrealistic that the 2.3‰ increase in ε_p was caused by slowing growth rates or decreasing cell sizes from values more than four times those that are typical of most modern environments, which would need to be sustained globally for millions of years during the Early Ordovician before decreasing during the Middle Ordovician.

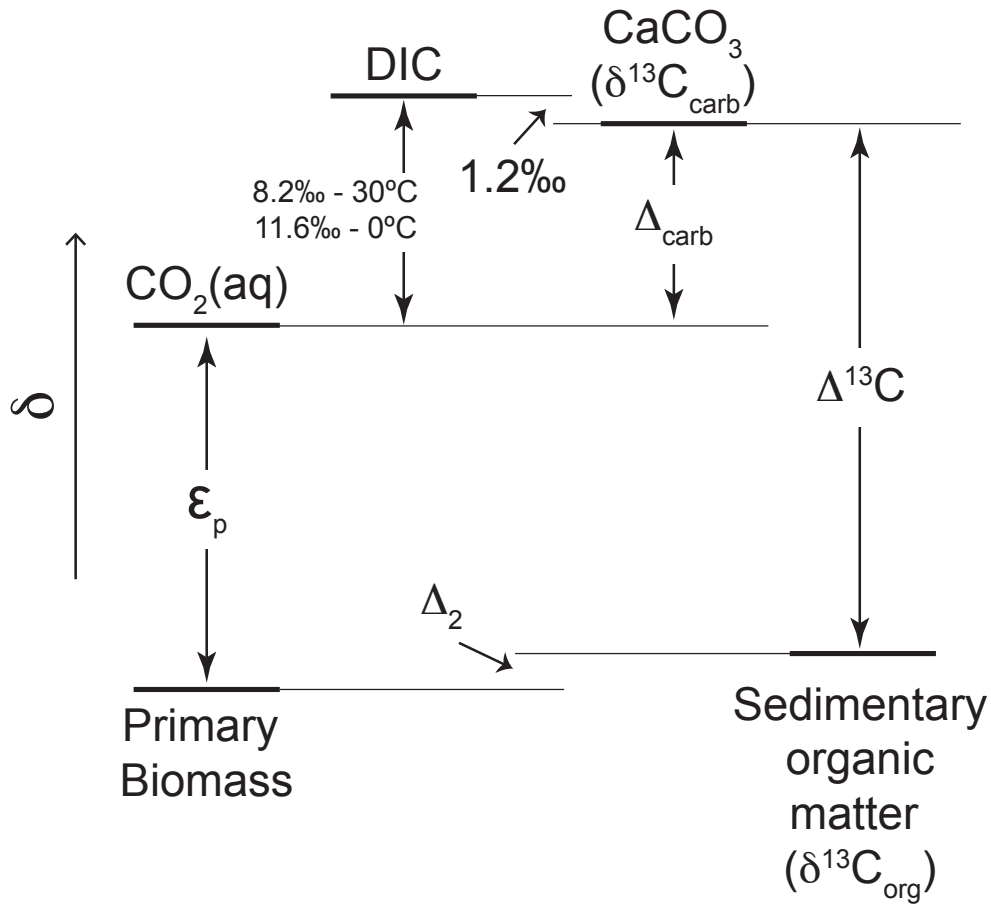

$$\Delta^{13}C = \varepsilon_p + \Delta_{carb} - \Delta_2$$

Edwards et al., Figure S7

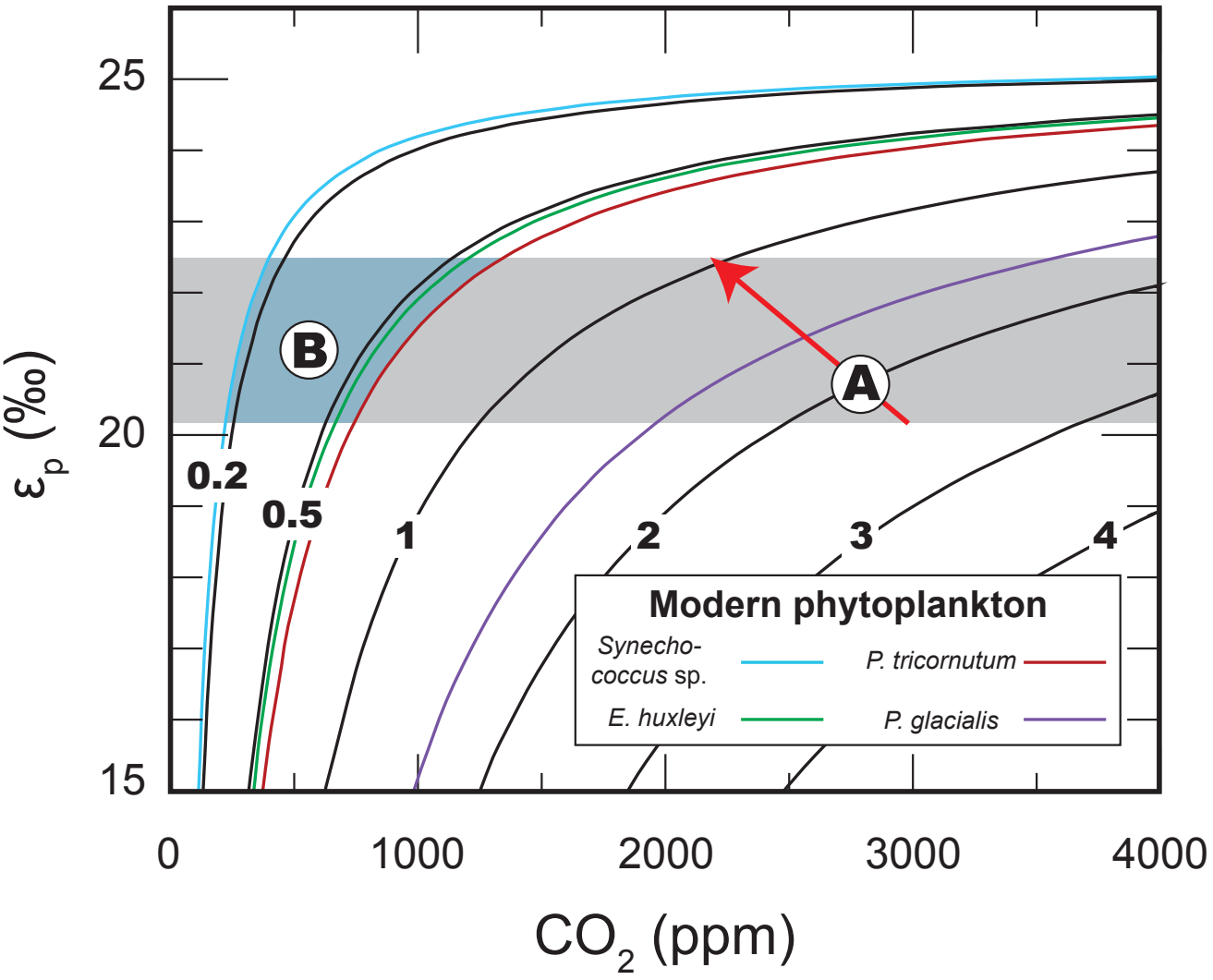

Edwards et al., Figure S8

193 *Determining Ordovician ε_p values*

194 Existing fossil evidence severely under-represents the true diversity of size and
195 shape of Ordovician phytoplankton, but some soft-bodied acritarchs (dinoflagellate cysts)
196 preserved in Silurian limestone are 5 to 10 μm in diameter[65] and similar in size to modern
197 planktic coccolithiphores and diatoms originally studied by Popp et al. (ref. 21). If
198 Ordovician seas were dominantly populated by small phytoplankton forms, of which
199 almost no evidence exists to confirm or refute this, factors such as carbon concentrating
200 mechanisms or other 'vital effects' could have affected ε_p and $\delta^{13}C_{org}$. It is also likely
201 that bulk $\delta^{13}C_{org}$ data used herein includes components of bulk organic matter from
202 different algal and bacterial assemblages, including benthic mat-forming algae and
203 cyanobacteria in addition to planktonic forms. However, because this dataset includes
204 data from several ocean basins that overlap in time, we assume that any anomalous $\varepsilon_{p\text{-}}$
205 $_{estimated}$ values due to algal assemblages, and not atmospheric O_2 change, will be averaged
206 out by the large dataset and LOESS smoothing line.
207
208 **Ordovician cooling based on conodont apatite $\delta^{18}O$:**

209 Trotter et al. (ref. *6*) inferred that global Ordovician ocean temperatures cooled
210 based on oxygen isotope ($\delta^{18}O$) paleothermometry from conodont apatite. Sampled
211 conodonts were collected from several sedimentary basins around the globe and from a
212 range of time bins in the Ordovician and Silurian. Each of these bins represents several
213 million years such that ten discrete time slices comprise the Early–Middle Ordovician.
214 Based on the observed $\delta^{18}O$ increase, sea surface temperatures were estimated to cool
215 from 41 ºC to 30 ºC during the Early to Middle Ordovician (Tremadocian–Darriwilian),

then cooling further to ~23 ºC by the end-Ordovician glaciation[6]. This cooling occurs at approximately the same time as the observed $\Delta^{13}C$ increase (Fig. 1). An 11ºC drop in surface ocean temperatures from 41 ºC would result in a 1.3‰ increase in the fractionation effect between DIC and carbonate formation (see above). This would translate into larger $\Delta^{13}C$ values (if Δ_2 remained constant) during the start of the cooling trend at the base of the Ordovician. Therefore in order to estimate changes in ε_p using the $\Delta^{13}C$ trend ($\delta^{13}C_{carb}$ and $\delta^{13}C_{org}$), temperature must be considered to account for the effect on the formation of carbonate as well as the solubility of CO_2 into seawater.

Sensitivity testing using an alternative equation[66] to calculate paleotemperature using conodont-based $\delta^{18}O$ data shows a similar O_2 trend as the standard run but with slightly higher O_2 estimates overall (Fig. S4C). This alternate O_2 trend also predicts that oxygenation occurred during the Middle–Late Ordovician. Further sensitivity testing using a constant $\delta^{18}O$ value for seawater of -3‰ instead of -1‰[6] used in the standard run shows a similar pattern where the timing of the oxygenation does not change but only the magnitude of O_2 levels (Fig. S4D).

Calculation of ε_p

Variations in both atmospheric O_2 and CO_2 can influence the fractionation effect produced by primary producers during photosynthesis[20,59,67,68]. This is because the RuBisCO enzyme (where the major fractionation effect occurs during carbon fixation) has a dual carboxylase-oxygenase function[59]. Increased atmospheric O_2 can produce larger ε_p values as observed in various groups of photosynthetic organisms. To solve for the size of the atmospheric oxygen reservoir we use estimates of ε_p using Eq. 1 of the

main text and $\delta^{13}C_{carb}$ and $\delta^{13}C_{org}$ data from Edwards and Saltzman (ref. 23) and new data (Fig. 1; Table S2) as $\delta^{13}C$ proxies of the DIC (δ_d, in the form of dissolved CO_2) and biomass (δ_p). $\delta^{13}C_{carb}$ can be used to solve for the $\delta^{13}C$ of dissolved CO_2 (δ_d) from the relationship (from ref. 31):

$$\delta_d = \delta^{13}C_{carb} - 1‰ + \varepsilon_{b(a)} \quad [S1]$$

where 1‰ (± 0.2‰) represents the ^{13}C enrichment associated with the formation of calcite from seawater[69], and $\varepsilon_{b(a)}$ = the temperature effect of $\delta^{13}C$ between dissolved CO_2 and HCO_3^- in seawater[70]. $\varepsilon_{b(a)}$ is calculated using the equation:

$$\varepsilon_{b(a)} = 24.12 + 9866/T \quad [S2]$$

where T = temperature in Kelvin, which we base on temperatures estimated from conodont apatite $\delta^{18}O$ (Table S2)[6].

To adjust for secondary alteration of the biomass (δ_p), we subtract 1.5‰ from $\delta^{13}C_{org}$ values:

$$\delta_p = \delta^{13}C_{org} - 1.5‰ \quad [S3]$$

based on the average offset between organic matter in the sediment compared to what has been measured in the overlying water column[25] (Δ_2). These δ_d and δ_p values can now be used to solve for ε_p using Eq. 2 of the main text.

Expected ε_p

Experimental studies[21,22] on modern phytoplankton (at fixed O_2 levels) show that the overall photosynthetic fractionation effect (ε_p) is a function of both biological factors (growth rate and cell geometry) and the concentration of dissolved CO_2 ($[CO_2]_{aq}$) (Eq. 2 of the main text). If the biological factors remain relatively constant for the

phytoplankton groups that make up the majority of biomass, then ε_p can be calculated based only on variations in $[CO_2]_{aq}$. To solve for $[CO_2]_{aq}$ we use the CO_2 results from GEOCARB and Henry's law:

$$[CO_2]_{aq} = K_o \times CO_2 \text{ (ppm)} \quad [S4]$$

where K_o is the solubility constant in seawater dependent on salinity (we use 35 ppt) and temperature[71] (Table S2). The difference between calculated ε_p (from $\Delta^{13}C$ data; Eq. 1) vs. expected ε_p (GEOCARB CO_2; Eq. 2) is assumed to reflect changes in atmospheric O_2 relative to our modern atmosphere, where negative values represent atmospheric O_2 levels less than the modern (21%) and vice versa for positive values (Fig. S3). We solve for the size of atmospheric O_2 reservoir (M_{O2}, 10^{18} mol) by rearranging Eq. 3:

$$M_{O2} = 38 \times ((\varepsilon_1 - \varepsilon_2) + J)/J \quad [S5]$$

where 38 represents the size of the modern atmospheric O_2 reservoir ($\times 10^{18}$ mol).

Biodiversity curves using the Paleobiology Database

The biodiversity curve used in this study (Fig. 3 of the main text) was constructed using data[72] from the Paleobiology Database (www.fossilworks.org) and methods similar to other biodiversity studies[73], producing a trend similar to others where brachiopods[39,40] and all taxa[1] diversity rapidly increased during the Middle Ordovician (Fig. S9). The database was queried to provide all taxa at the genus taxonomic rank that had been entered at the time of acquisition (June 2015) extant between ages between 510 Ma and 430 Ma (this is to avoid edge effects when looking at biodiversity trends during the Ordovician: 490–440 Ma). Our diversity curve is constructed using first and last occurrences of taxa (without singletons[74]) and time bins of 1 Myr. For time bins where

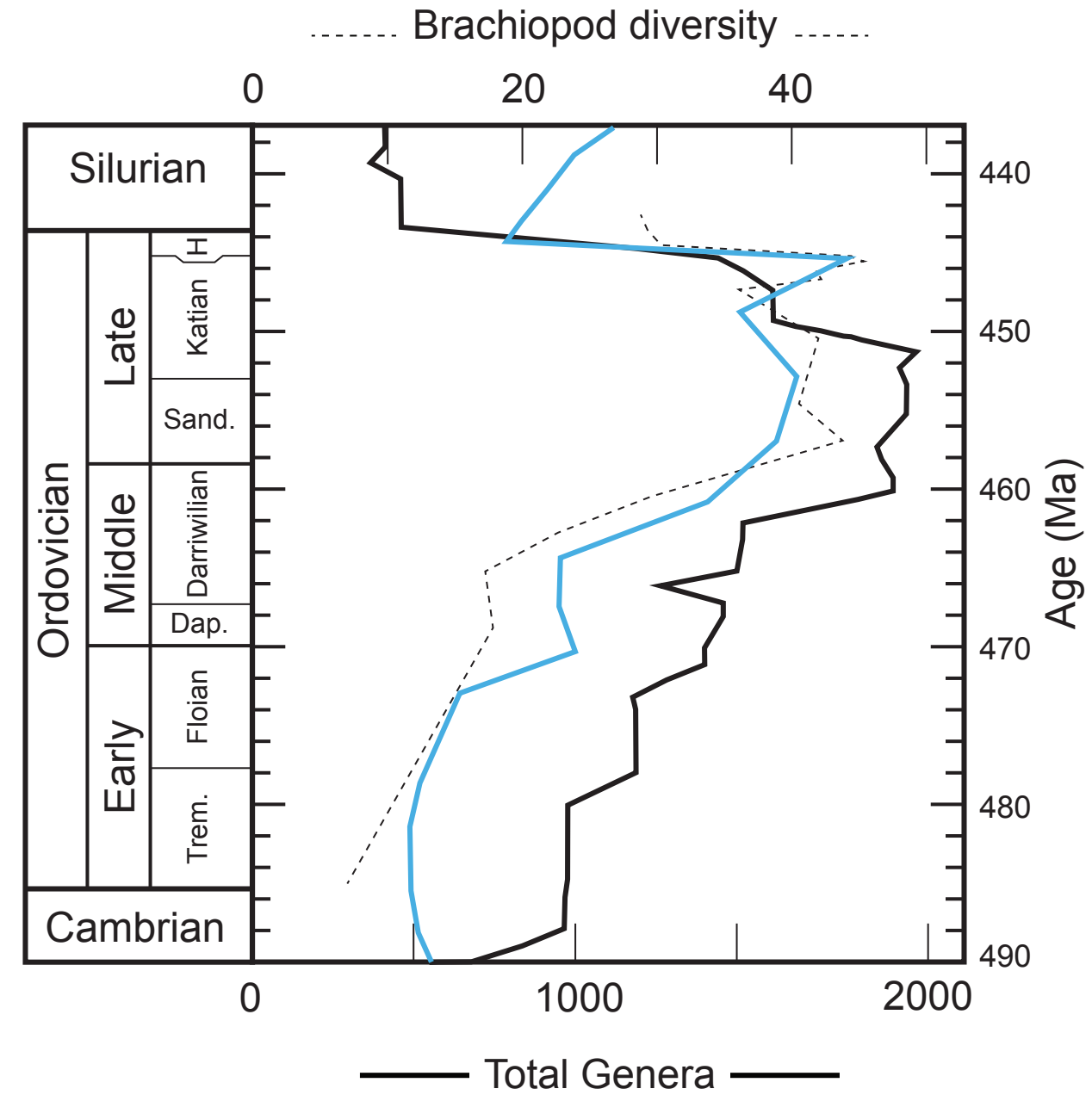

Edwards et al., Figure S9

285 taxa have either a first or last occurrence half a unit is assigned for that time bin, whereas
286 bins receive a full unit where taxa range through the entire time bin.
287 The new curve has improved age resolution compared to some of the original
288 work of Sepkoski (ref. 1 and refs. therein) as well as incorporating taxonomic
289 occurrences on a more global scale. This curve relies less on the fossil record described
290 from the intensely studied carbonate strata that were deposited under epicontinental seas
291 covering Laurentia that may not be representative of marine ecosystems globally[4].
292 Several assumptions and biases are inherent in interpreting trends using this kind of
293 database (e.g. sampling and preservation, reported fossil occurrences that have not yet
294 been entered, poor age assignments), but these errors are thought to be random and do not
295 significantly change biodiversity trends when thoroughly screened[75] (this approach was
296 not conducted in this study). Incorrect taxonomic identification in the Sepkoski
297 compendium has been shown to be non-random among Ordovician and Silurian crinoid
298 genera[76]; however, the corrected compilation made by Ausich and Peters (ref. 76) shows
299 the same overall trend in biodiversity. Because the scope of this study is to compare the
300 overall trend in Ordovician biodiversity with atmospheric O_2, we do not consider that
301 errors resulting from incorrect taxonomic identification would drastically change our
302 conclusions. We use the generic taxonomic level instead of species to minimize
303 overestimates of actual biodiversity that might result from ambiguous species
304 assignment[4] or poor preservation of some species-specific morphologic structures.
305 A total of 5335 different genera from 94,177 occurrences were used (Table S4).
306 The dataset was checked to remove errors, often identified as a single occurrence, such as
307 trace fossils (ichnogenera, n=17) and spelling mistakes (n=208), both of which would

result in overestimates of actual diversity. Spelling errors occur either as mistakes made by the original author, which were entered into the database as originally reported, or as transcription errors during database entry. Despite this thorough vetting process there were still 73 entries (out of 94,177) that could not be verified, and removing them from the overall database made no noticeable change in the overall biodiversity curve. The taxonomic affiliation of these unverified entries was assigned based on likely groups from the Latin derivatives of their generic name, and if doubt remained they were listed as 'unclassified' when assigning them to one of the three evolutionary faunas.

SUPPLEMENTAL REFERENCES

50. Bergström, S. M., Young, S. & Schmitz, B. Katian (Upper Ordovician) $\delta^{13}C$ chemostratigraphy and sequence stratigraphy in the United States and Baltoscandia: A regional comparison. *Palaeogeogr. Palaeoclimatol. Palaeoecol.* **296,** 217–234 (2010).

51. Gouldey, J. C., Saltzman, M. R., Young, S. A. & Kaljo, D. Strontium and carbon isotope stratigraphy of the Llandovery (Early Silurian): Implications for tectonics and weathering. *Palaeogeogr. Palaeoclimatol. Palaeoecol.* **296,** 264–275 (2010).

52. Laporte, D. F. *et al.* Local and global perspectives on carbon and nitrogen cycling during the Hirnantian glaciation. *Palaeogeogr. Palaeoclimatol. Palaeoecol.* **276,** 182–195 (2009).

53. Young, S. A., Saltzman, M. R., Bergström, S. M., Leslie, S. A. & Xu, C. Paired $\delta^{13}C_{carb}$ and $\delta^{13}C_{org}$ records of Upper Ordovician (Sandbian – Katian) carbonates in North America and China: Implications for paleoceanographic change. *Palaeogeogr. Palaeoclimatol. Palaeoecol.* **270,** 166–178 (2008).

54. Buggisch, W., Keller, M. & Lehnert, O. Carbon isotope record of Late Cambrian to Early Ordovician carbonates of the Argentine Precordillera. *Palaeogeogr. Palaeoclimatol. Palaeoecol.* **195,** 357–373 (2003).

55. Azmy, K. & Lavoie, D. High-resolution isotope stratigraphy of the Lower Ordovician St . George Group of western Newfoundland , Canada: implications for global correlation. *Can. J. Earth Sci.* **423,** 403–423 (2009).

56. Pancost, R. D., Freeman, K. H. & Patzkowsky, M. E. Organic-matter source

variation and the expression of a late Middle Ordovician carbon isotope excursion. *Geology* **27,** 1015–1018 (1999).

57. Metzger, J. G. & Fike, D. A. Techniques for assessing spatial heterogeneity of carbonate $\delta^{13}C$ values: Implications for craton-wide isotope gradients. *Sedimentology* **60,** 1405–1431 (2013).

58. Saltzman, M. R. *et al.* Pulse of atmospheric oxygen during the late Cambrian. *Proc. Natl. Acad. Sci. U. S. A.* **108,** 3876–3881 (2011).

59. Beerling, D. J. *et al.* Carbon isotope evidence implying high O_2/CO_2 ratios in the Permo-Carboniferous atmosphere. *Geochim. Cosmochim. Acta* **66,** 3757–3767 (2002).

60. Gomes, M. L., Hurtgen, M. T. & Sageman, B. B. Biogeochemical sulfur cycling during Cretaceous oceanic anoxic events: A comparison of OAE1a and OAE2. *Paleoceanography* **31,** 233–251 (2016).

61. Owens, J. D. *et al.* Sulfur isotopes track the global extent and dynamics of euxinia during Cretaceous Oceanic Anoxic Event 2. *Proc. Natl. Acad. Sci. U. S. A.* **110,** 18407–18412 (2013).

62. Bolton, C. T. & Stoll, H. M. Late Miocene threshold response of marine algae to carbon dioxide limitation. *Nature* **500,** 558–562 (2013).

63. Bolton, C. T., Stoll, H. M. & Mendez-Vicente, A. Vital effects in coccolith calcite : Cenozoic climate-pCO_2 drove the diversity of carbon acquisition strategies in coccolithophores? *Paleoceanography* **27,** PA4204 (2012).

64. Kodina, L. A., Bogacheva, M. P., Lyutsarev, S. B. Particulate organic carbon in the Black Sea: isotopic composition and origin. *Geochemistry Int.* **34,** 798–804

(1996).

65. Munnecke, A. & Servais, T. Scanning electron microscopy of polished, slightly etched rock surfaces: a method to observe palynomorphs *in situ*. *Palynology* **20,** 163–176 (1996).

66. Pucéat, E. *et al.* Revised phosphate-water fractionation equation reassessing paleotemperatures derived from biogenic apatite. *Earth Planet. Sci. Lett.* **298,** 135–142 (2010).

67. Fletcher, B. J., Brentnall, S. J., Quick, W. P. & Beerling, D. J. BRYOCARB: A process-based model of thallose liverwort carbon isotope fractionation in response to CO_2, O_2, light and temperature. *Geochim. Cosmochim. Acta* **70,** 5676–5691 (2006).

68. Tappert, R. *et al.* Stable carbon isotopes of C3 plant resins and ambers record changes in atmospheric oxygen since the Triassic. *Geochim. Cosmochim. Acta* **121,** 240–262 (2013).

69. Romanek, C. S., Grossman, E. L. & Morse, J. W. Carbon isotopic fractionation in synthetic aragonite and calcite: Effects of temperature and precipitation rate. *Geochim. Cosmochim. Acta* **56,** 419–430 (1992).

70. Mook, W. G., Bommerson, J. C. & Staverman, W. H. Carbon isotope fractionation between dissolved bicarbonate and gaseous carbon dioxide. *Earth Planet. Sci. Lett.* **22,** 169–176 (1974).

71. Weiss, R. F. Carbon dioxide in water and seawater: the solubility of a non-ideal gas. *Mar. Chem.* **2,** 203–215 (1974).

72. Wagner, P., Kröger, B., Holland, S., Kiessling, W., Miller, A., Patzkowski, M.,

Hopkins, M. Taxonomic occurrences recorded in Fossilworks and the Paleobiology Database. *Fossilworks* (2015). Available at: fossilworks.org.

73. Hammer, Ø. & Harper, D. A. T. *Paleontological Data Analysis*. *Paleontological Data Analysis* (2007). doi:10.1002/9780470750711

74. Foote, M. Origination and extinction components of taxonomic diversity: general problems. *Paleobiology* **26,** 74–102 (2000).

75. Smith, A. B. Large-scale heterogeneity of the fossil record: implications for Phanerozoic biodiversity studies. *Philos. Trans. R. Soc. B Biol. Sci.* **356,** 351–367 (2001).

76. Ausich, W. I. & Peters, S. E. A revised macroevolutionary history for Ordovician – Early Silurian crinoids. *Paleobiology* **31,** 538–551 (2005).

SUPPLEMENTAL FIGURES

Figure S1. Atmospheric CO_2 and O_2 estimates using GEOCARB, comparing results between a previously published run[33] and this study with a 5 Myr time-step and new carbon, sulfur, and strontium isotope data.

Figure S2. Sensitivity testing of new isotope data used in the GEOCARB approach. Each parameter (colored symbols) is held constant, starting at the 490 Myr time bin, and compared with the standard run (red squares, from Fig. 2). The mid-Ordovician CO_2 drop is seen among all model runs, particularly with a constant $\delta^{13}C$, suggesting that a combination of parameters is responsible for this drop. The mid-Ordovician O_2 drop in the standard run is reproduced when $\delta^{13}C$ and $^{87}Sr/^{86}Sr$ values are constant, indicating that this O_2 drop is driven by the $\delta^{34}S$ record. However, the Middle–Late Ordovician O_2 increase is reproduced in the constant $\delta^{34}S$ run but not in the constant $\delta^{13}C$ run, indicating that this increase is driven by the $\delta^{13}C$ record. Constant $^{87}Sr/^{86}Sr$ values seems to have no appreciable difference on atmospheric O_2 compared to the standard run.

Figure S3. Estimates of atmospheric CO_2 (left) and ε_p (right) using $\delta^{13}C$ data and GEOCARB model results. Atmospheric CO_2 from GEOCARB (yellow line) is compared with expected CO_2 (black line) using calculated ε_p values (from the black line in the right panel, which represents a smoothed LOESS line of $\varepsilon_{p\text{-estimated}}$ using $\Delta^{13}C$ data presented in Figure 1,which have been adjusted for temperature effects), and Eq. 2. The difference between these trends suggests that some factor other than CO_2 played a role in the

fractionation of ^{13}C into biomass. Solving for expected ε_p using CO_2 from GEOCARB, adjusted for temperature effects, and Eq. 2 (yellow line in the right panel) shows a similar relationship where there is a mismatch between expected and estimated ε_p. This mismatch is interpreted here as the effect of O_2 on the fractionation effect imparted by RuBisCO[20] and the difference between the trends (gray regions) reflects changes in atmospheric O_2 compared to modern levels (21%).

Figure S4. Sensitivity tests of atmospheric O_2 model estimates using the photosynthetic fractionation approach by A) varying the dependence of O_2 on fractionation (J parameter in Eq. 3), B) using atmospheric CO_2 estimates from the COPSE model[13] and constant high and low CO_2 levels, C) using a different equation used to estimate temperature from phosphate oxygen isotopes[66] and assuming a constant sea surface temperature of 27 ºC, and D) using an average $\delta^{18}O$ value of -3‰ for seawater instead of -1‰ used in the standard run.

Figure S5. Calculated atmospheric O_2 values for paired $\delta^{13}C$ values (Table S2) using the photosynthetic fractionation effect approach, with LOESS smoothed line of mean atmospheric O_2 values and 95% CI envelope from Fig. 2 (not the error associated with each data point; see supplement for further discussion). Large blue circles represent averaged values in 5 Myr bins for comparison of O_2 trends made using data at 5 Myr (e.g. GEOCARB).

Figure S6. Late Ordovician (Hirnantian) $\delta^{13}C$ data used to estimate O_2 using the photosynthetic fractionation approach. Data from Anticosti Island (green triangles and blue diamonds) show a slight increase in $\delta^{13}C_{org}$ prior to the positive $\delta^{13}C_{carb}$ excursion known as the HICE event. This decrease in the difference between the reservoir ($\delta^{13}C_{carb}$) and biomass ($\delta^{13}C_{org}$) is expressed as a decrease in atmospheric O_2 using the O_2-dependent approach. $\delta^{13}C$ data from Nevada (red squares) also predict a decrease in atmospheric O_2 (black arrow), but graptolite biostratigraphic information used to assign ages to these data may be incomplete and give the appearance of two O_2 drops (one at 444.84 Ma and one at 444.80 Ma) that may in fact record the same O_2 crisis prior to the HICE.

Figure S7. Schematic diagram of the isotopic relationships involved in the production of sedimentary organic matter from seawater. Modified from Hayes et al. (ref. 25).

Figure S8. Relationship between atmospheric CO_2 concentration (ppm) and the isotopic fractionation (ε_p) imparted during primary production at varying growth rates (μ; black contoured lines) at V/S = 1 μm. Examples of modern phytoplankton are shown in colored lines[22]. Gray region shows range of possible ε_p increase from 20.2‰ to 22.5‰ (Fig. S3). Red arrow (A) represents overall trend of atmospheric CO_2 estimates from GEOCARB during the observed increase in ε_p, which requires unrealistic μ or V/S values far higher than modern phytoplankton. The light blue region (B) represents range of growth conditions typical of modern small phytoplankton likely present during the Ordovician (*P. glacialis* is considered a large diatom compared to the others listed[22]), but

in order for ε_p to increase from 20.2‰ to 22.5‰ atmospheric CO_2 would have to increase from levels significantly lower than CO_2 model estimates. *E. huxleyi* = *Emiliania huxleyi*, *P. tricornutum* = *Phaeodactylum tricornutum*, *P. glacialis* = *Porosira glacialis*.

Figure S9. Comparison of biodiversity curves of all marine taxa (solid lines) from this study (black) and a recent compilation (blue[1]), and global brachiopod diversity (dashed black line[39]).

Table S1. Binned isotope data* used for GEOCARB and model results of O_2 and CO_2 with error estimates.

Table S2. Isotope data and atmospheric O_2 using the photosynthetic fractionation effect approach.

Table S3. New $\delta^{13}C^*$ and $\delta^{34}S$ data# used in the photosynthetic fractionation effect and GEOCARB models.

Table S4. Taxonomic data* used to construct the biodiversity curve (Fig. 3) with Evolutionary Faunas, First Appearance Datum (FAD), and Last Appearance Datum (LAD).

Table S5. Example calculations for error propagation using the O_2-dependent photosynthetic fractionation approach.